Journal of Asian Earth Sciences 209 (2021) 104683

Contents lists available at ScienceDirect

Journal of Asian Earth Sciences

journal homepage: www.elsevier.com/locate/jseaes

Liquid immiscibility in the Panzhihua intrusion, SW China: Evidence from ore textures and Fe–Ti oxide-rich globules in gabbros

Feng Xiong [a,b], Yan Tao [a,*], Mingyang Liao [c], Yuqi Liao [a,b], Jun Ma [a,b]

[a] State Key Laboratory of Ore Deposit Geochemistry, Institute of Geochemistry, Chinese Academy of Sciences, Guiyang 550081, China
[b] University of Chinese Academy of Sciences, Beijing 100049, China
[c] Institute of Mining Engineering, Guizhou Institute of Technology, Guiyang 550003, China

ARTICLE INFO

Keywords:
Liquid immiscibility
Panzhihua layered intrusion
Magmatic Fe–Ti oxide deposit
Emeishan large igneous province

ABSTRACT

The Panzhihua intrusion hosts a large Fe–Ti oxide deposit in the Permian Emeishan large igneous province (ELIP), SW China. The mechanism of such massive Fe–Ti oxide accumulation in the layered intrusion is still a matter of debate. In this study, we suggest that the ore formation occurred via density-driven liquid segregation of immiscible Fe-rich liquid, instead of simple mineral sorting of Fe–Ti oxides. Interstitial oxides and kinked plagioclase crystals reveal that the Fe–Ti oxides were crystallized in-situ after their surrounding silicate minerals. Dissolution texture of primocryst plagioclase is ubiquitous in the ores, indicating that the primocryst plagioclase grains were in disequilibrium with the surrounding melt. Fe–Ti oxide-rich globules (~38 wt% FeO) are present in the ore-barren gabbro, and likely represent solidified pockets of the immiscible Fe-rich liquid. Olivine in the Fe–Ti oxide ores occurs as primocrysts (avg. Fo = 68.5) that crystalized before the interstitial Fe–Ti oxides, or as growth rims (avg. Fo = 77.5) that crystalized after interstitial Fe–Ti oxides. The primocryst olivine was likely in equilibrium with the Panzhihua parental magma, and its composition matches well with that of the basalt ($Fe_2O_3^T$ = ~16 wt%) exposed near the intrusion. The olivine rim was likely in equilibrium with the residual melt produced from ~33% crystallization of the Fe–Ti oxide-rich globule. This study confirms that the ore layers are formed by the sinking of dense immiscible Fe-rich liquid to squeeze out the original silicate melt in the crystal mush, forming the (semi-)massive Fe–Ti oxide layered ores.

1. Introduction

Liquid immiscibility in basaltic magmas is a contentious issue (Philpotts, 1982, Philpotts and Doyle, 1983; Veksler, 2009; Veksler et al., 2007; Charlier et al., 2013; Lindsley and Epler, 2017), and includes a number of long-standing petrological disputes, notably the basaltic magma evolution trend, such as Daly gap (Charlier et al., 2011), and the formation of various layered intrusions (e.g., Skaergaard, Sept Iles, Duluth, Bushveld), which hold the key to the origin of Fe–Ti oxide deposits (Namur et al., 2012).

Many studies have identified immiscibility between Fe-rich and Si-rich liquids in the evolved ferrogabbros from many layered intrusions, such as Skaergaard (Holness et al., 2011; Humphreys 2011; Jakobsen et al., 2005, 2011), Sept Iles (Charlier et al., 2011), Duluth (Ripley et al., 1998) and Bushveld (Vantongeren and Mathez 2012; Fischer et al., 2016). Based on late-stage microstructures, Holness et al. (2011) suggested that liquid immiscibility could occur in the crystal-mush to generate late-stage granophyres at Skaergaard. Philpotts (2008) and McBirney (2008) suggested that the two-liquid field does not extend stably above 1040 °C in fractionated basaltic magmas, and thus liquid immiscibility can only generate late-stage granophyres from fractionated tholeiitic magmas. In contrast, Kamenetsky et al. (2013) suggested that large-scale, continuous magma immiscibility can occur after the cooling of magma chambers, as supported by the coexisting silica-rich/-poor melt droplets from the Siberian trap.

Experimental studies by Charlier and Grove (2012) show that immiscibility could occur below 1040 °C, and can therefore play a fractionation role of basaltic magma only during the late magmatic stages. This implies that immiscibility cannot generate Fe–Ti oxide mineralization. However, experimental studies by Veksler et al. (2007) and Hou and Veksler (2015) demonstrated that immiscibility can occur in fractionating basaltic magma at above 1100 °C (i.e., at much earlier

* Corresponding author at: State Key Laboratory of Ore Deposit Geochemistry, Institute of Geochemistry, Chinese Academy of Sciences, Guiyang, Guizhou Province 550081, China.
E-mail address: taoyan@vip.gyig.ac.cn (Y. Tao).

https://doi.org/10.1016/j.jseaes.2021.104683
Received 24 June 2020; Received in revised form 15 January 2021; Accepted 16 January 2021
Available online 27 January 2021

magmatic stages), and can thus form Fe–Ti oxide mineralization.

As a world-renowned magmatic Fe–Ti oxide deposit, the Panzhihua intrusion had received much research attention (Zhou et al., 2005, 2013; Pang et al., 2008, 2013; Howarth et al., 2013; Song et al., 2013), but the mechanism to accumulate large amounts of Fe–Ti oxides in the layered intrusions is still under debate. Major metallogenic models fall into two categories: liquid immiscibility or Fe–Ti oxides crystallization from the parental basaltic magma. Based on the ore textural and petrologic study, Zhou et al. (2013) and Wang and Zhou (2013) proposed a model involving segregation of Fe–Ti-rich liquids from the gabbroic magmas, but Pang et al. (2008) and Song et al. (2013) argued that the oxide ores were formed by settling and density-sorting of early-crystallized Fe–Ti oxides minerals. Here, we report new evidence of liquid immiscibility from the ore textures and rock-forming mineral features, which support a liquid-immiscibility model for Panzhihua.

2. Geological background

In the western Yangtze block, the Permian Emeishan large igneous province (ELIP) magmatism has led to extensive emplacement of flood basalts and mafic–ultramafic intrusions (Fig. 1). The ELIP basalts cover an area of about 3×10^5 km^2, with thickness ranging from several hundred meters up to 5 km. The ELIP magmatism has been interpreted to be mantle plume-related (Xu et al., 2001, 2004; Zhou et al., 2002). The volcanic succession is underlain by limestone of the Middle Permian Maokou Formation (Fm.), and overlain by shale and volcaniclastic rocks of the Upper Permian Xuanwei Fm. The ELIP mafic–ultramafic intrusions are mainly exposed in the western Yangtze block, along a belt that extends from Panzhihua-Xichang to the Ailaoshan-Red River fault (Fig. 1). Zircon U-Pb dating of these intrusions yielded ages of ca. 260 Ma (Zhou et al., 2002, 2008; Tao et al., 2009; Zhong and Zhu, 2006; Zhong et al., 2011; Liu et al., 2020).

Two types of ore deposits are associated with the ELIP mafic–ultramafic intrusions: Ni–Cu–PGE sulfide deposits in small and more-primitive intrusions (Song et al., 2003, 2008; Zhou et al., 2008; Wang et al., 2018a; Li et al., 2019), and Fe–Ti–V oxide deposits in larger and more-evolved intrusions (Zhou et al., 2005, 2013; Wang et al., 2008; Wang and Zhou, 2013; Pang et al., 2008, 2013; Zhang et al., 2009; Hou et al., 2012; Song et al., 2013; Liao et al., 2015, 2016; Yu et al., 2015; Chen et al., 2017; Bai et al., 2019).

Occurrence of magmatic Fe–Ti oxide deposits (e.g., Panzhihua, Hongge, Baima, Taihe, and Xinjie) in the ELIP layered intrusions is controlled by major N–S trending faults (Fig. 1). The ore-bearing intrusions are spatially associated with contemporaneous flood basalts and granitoids. The four largest Fe–Ti oxide deposits (i.e., Panzhihua, Hongge, Baima, and Taihe) host a total ore reserve of ~7.209 billion tonnes (Gt) total Fe, ~559 million tonnes (Mt) TiO_2, and ~17.4 Mt V (Ma et al., 2003).

3. Panzhihua intrusion and Fe–Ti oxide deposit

The Panzhihua layered gabbroic intrusion (19 km long, 2 km thick) is emplaced into limestone, gneiss, and schist wallrocks (Fig. 2). The layered intrusion contains several fault-bounded ore segments

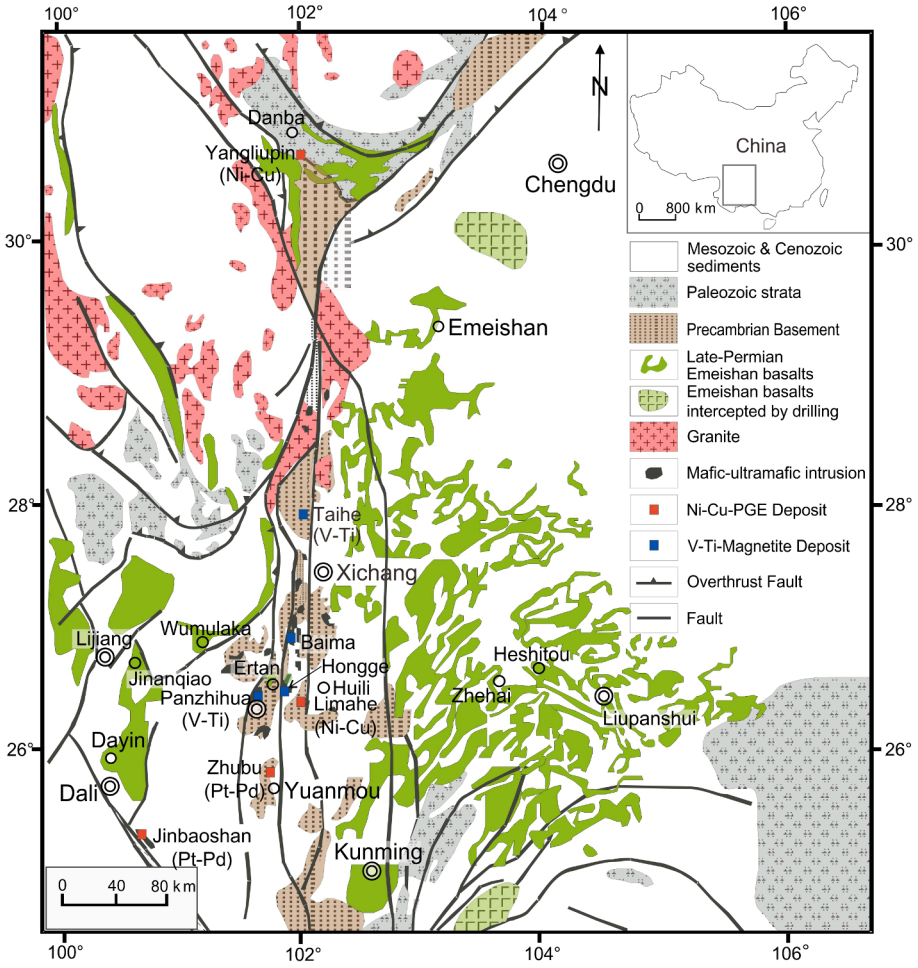

Fig. 1. Distribution of Permian flood basalts and coeval mafic–ultramafic intrusions in the Emeishan large igneous province (modified after Tao et al., 2015 and references therein).

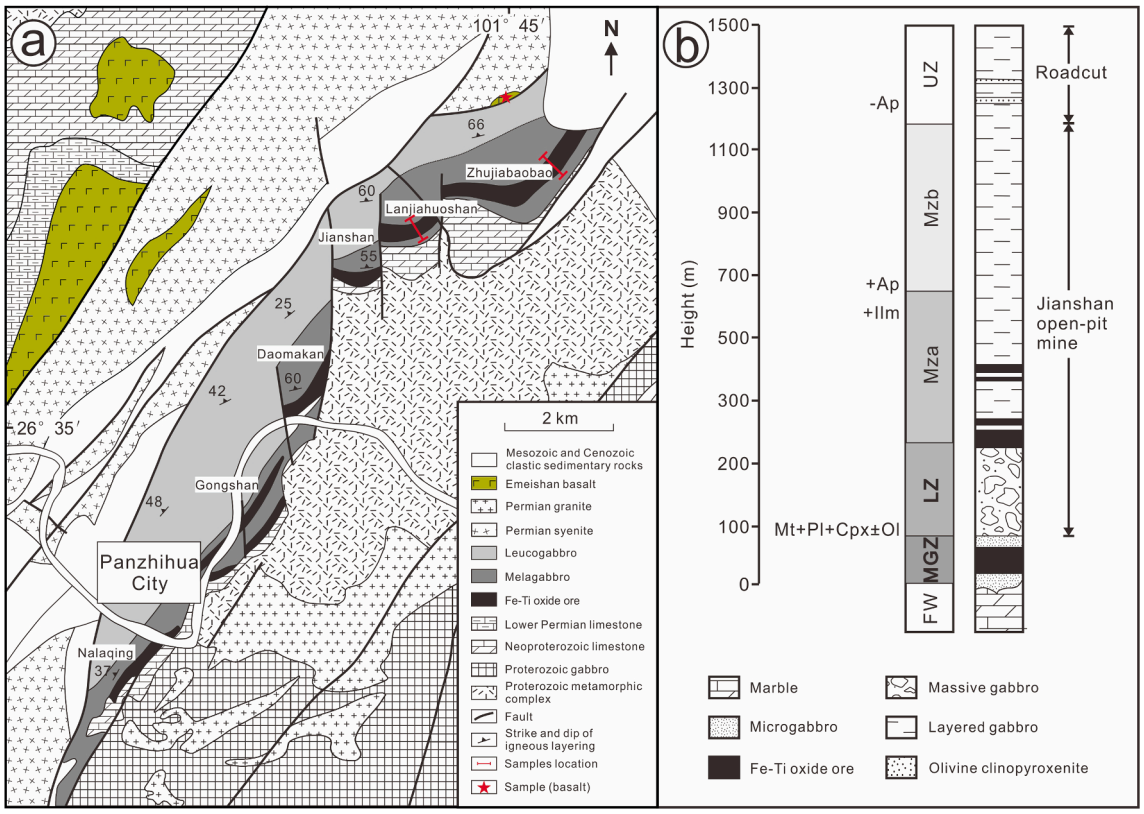

Fig. 2. (a) Geologic map of the Panzhihua intrusion, SW China (modified after Zhou et al., 2005), (b) The figure denotes an idealized stratigraphic column of the Jianshan segment of the Panzhihua intrusion (modified after Pang et al., 2009).

(Zhujiabaobao, Lanjiahuoshan, Jianbaobao, Daomakan, Gongshan, Nongnongping, and Nalaqing) along strike, and is composed of four lithological zones: Marginal Zone (MGZ), Lower Zone (LZ), Middle Zone (MZ) and Upper Zone (UZ) (Zhou et al., 2005; Pang et al., 2008). The MGZ (<40 m thick) is dominated by equigranular fine-grained gabbros with minor hornblende gabbros. The LZ (main ore-host, up to 110 m thick) consists mainly of gabbros, Fe–Ti-oxide gabbros and Fe–Ti-oxide ores. The Fe–Ti-oxide ores consist of (semi-)massive Fe–Ti oxides interstitial among olivine, clinopyroxene, and plagioclase. The MZ (up to 800 m thick) comprises leucogabbros and Fe–Ti-oxide gabbros. The UZ (500–1500 m thick) is mainly composed of layered gabbros and leucogabbros, with minor olivine clinopyroxenite and anorthosite (Fig. 2). The thickness of each zone varies significantly along strike (Fig. 2). The MGZ is present only in the NE segments (Zhujiabaobao, Lanjiahuoshan, and Jianbaobao) (Tang et al., 2017).

4. Petrography and Fe–Ti oxide ore textures

4.1. Petrography

The ore petrography was described by many studies (e.g., Zhou et al., 2005, 2013; Pang et al., 2008, 2013; Wang and Zhou, 2013). The ores contain varying amounts of Fe–Ti oxides, and can be classified into massive (Fe–Ti oxides > 60%), net-textured (Fe–Ti oxides = 20 to 60%), and disseminated (Fe–Ti oxides < 20%) (c.f. Wang and Zhou, 2013). In this study, net-textured ores and disseminated ores are also termed as Fe–Ti-oxide gabbros (Fig. 3).

Massive ores typically contain varying amounts of sparsely-isolated clinopyroxene, plagioclase, and olivine grains (Fig. 3a). Plagioclase grains show distinct dissolution features, whilst olivine growth rims were observed around clinopyroxene/plagioclase primocrysts, in contact with the interstitial Fe–Ti oxides. Clinopyroxene grains are typically Fe–Ti-rich, and contain two sets of titanomagnetite (minor ilmenite) exsolution lamellae along the crystal cleavages. As discribled by Zhou et al. (2005), the massive layered orebodies have sharp contact with the footwall. In some cases, the massive ores are transitional downward to disseminated ores, and then eventually to unmineralized gabbros.

Net-textured and disseminated ores are generally coarse-grained and consist of <20–60% Fe–Ti oxides, 20–30% clinopyroxene, 30–40% plagioclase, and minor (<5%) olivine (Fig. 3b and c). The net-textured ores are transitional to disseminated ores with decreasing concentration of interstitial Fe–Ti oxides. Olivine rims are observed around the clinopyroxene/plagioclase primocrysts, and isolate these primocrysts from the interstitial Fe–Ti oxides. Many plagioclase grains in the ores are found to be bended. It is widely seen that silicate minerals in the ores, especially plagioclase have resorption textures. Plagioclase primocrysts are dissolved to form embayment, which is in-filled with Fe–Ti oxides. Clinopyroxene contains ilmenite exsolution lamellae along the prismatic cleavage.

Unmineralized gabbro in the Lower and Middle zone are melagabbro, as described by Zhou et al. (2005). The gabbros are dark, and fine-grained (0.2–0.5 mm) equigranular (Fig. 3d). The rocks are composed generally of ~50 vol% clinopyroxene, ~40 vol% plagioclase, and minor (<5 vol%) magnetite and hornblende with/without olivine. Minor olivine grains occur locally as phenocrysts, whilst the interstitial magnetite is generally anhedral.

4.2. Fe–Ti oxides and silicates in the ores

4.2.1. Interstitial oxide and bent plagioclase

As shown in Figs. 4–6, Fe–Ti oxides are interstitial among silicate minerals in the Fe–Ti oxide ores of the Lower Zone, or as in-fill inside the eroded embayment of primocryst plagioclase. All these textural features demonstrate an intercumulus origin for the Fe–Ti oxides.

Crystal bending textures, e.g., deformation twinning and dislocation creep, were observed in plagioclase grains (Fig. 5), probably caused by

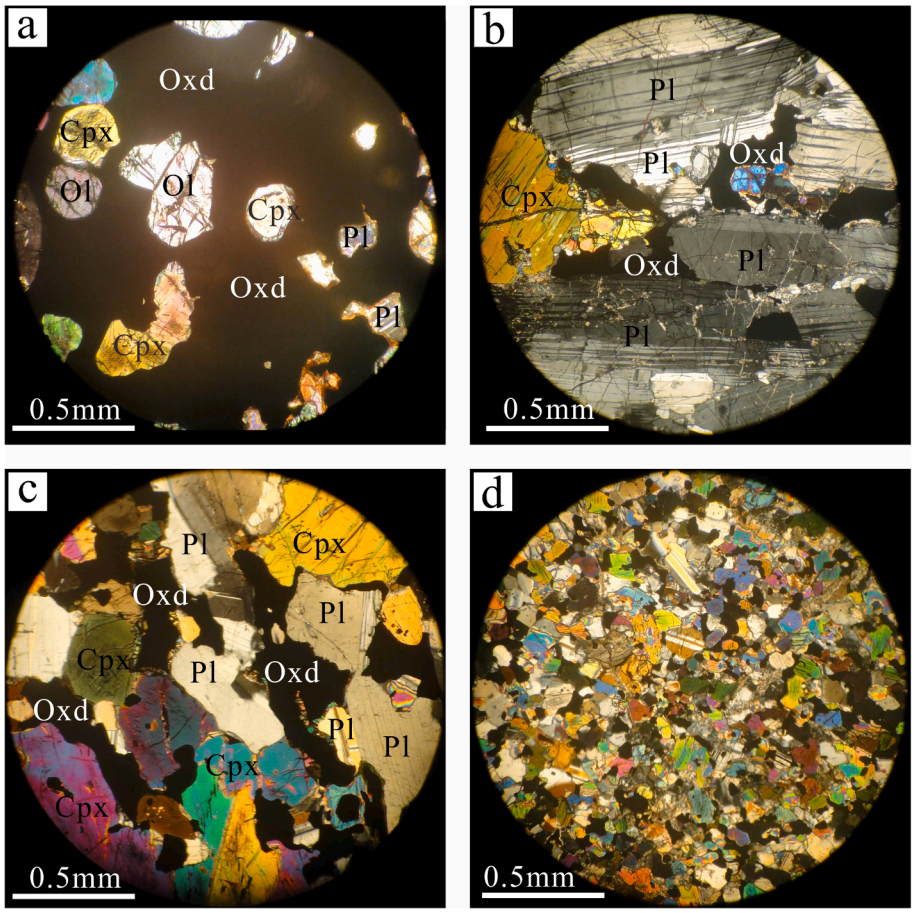

Fig. 3. Representative photomicrographs (crossed polar) of ores and gabbroic rocks from the Panzhihua intrusion: (a) massive ore with sparsely-isolated grains of clinopyroxene, plagioclase and olivine. Plagioclase shows dissolution texture; (b) net-textured ore with Fe–Ti oxides interstitial among clinopyroxene, plagioclase, and minor olivine; (c) disseminated ore with minor Fe–Ti oxides interstitial among clinopyroxene, plagioclase, and olivine. Olivine also occurs as growth rims around clinopyroxene and plagioclase, in contact with the interstitial Fe–Ti oxides; (d) ore-barren gabbro (Lower Zone) consists of equigranular clinopyroxene and plagioclase, and minor Fe–Ti oxide pockets. Abbreviations: Oxd-Fe–Ti oxide; Pl-plagioclase; Cpx-clinopyroxene; Ol-olivine.

loading from the crystal mush above (Philpotts AR and Philpotts DE, 2005; Holness et al., 2017). The Fe–Ti oxides are intercumulus and filled in the interstitial space of the crystal mush.

4.2.2. *Partially-dissolved plagioclase*

Dissolution texture of plagioclase is common in the ores (Fig. 6). Plagioclase primocrysts are eroded to form embayment and filled with Fe–Ti oxides. Such texure is also reported in the plagioclase from the Panzhihua intrusion and other layered intrusions in the Panxi region (Zhou et al., 2005; Wang and Zhou, 2013; Liu et al., 2016; Xing et al., 2017).

4.2.3. *Olivine rims*

There are two modes of olivine occurrence in the ores (Figs. 7 and 8): (1) granular olivine primocrysts crystallized with plagioclase and clinopyroxene primocrysts before the interstital Fe–Ti oxides; (2) olivine growth rim around clinopyroxene/plagioclase primocrysts, in contact with the interstitial Fe–Ti oxides. Olivine rims include polycrystalline and monocrystalline types, similar to those reported in the Skaergaard intrusion (Holness et al., 2011). The olivine rims was likely crystallized in late stage associated with Fe–Ti oxides crystallization.

4.2.4. *Fe–Ti oxide-rich globules*

Fe–Ti oxide-rich globules are hosted in the ore-barren gabbro sample PZH1, which is located above the massive oxide ore layer in the Lower Zone (Fig. 9). These globules (diameter: 1–2 mm) contain aggregates of Fe–Ti oxides (23 vol% magnetite and 12 vol% ilmenite) and silicate minerals (e.g., 50 vol% clinopyroxene, 8 vol% orthopyroxene, and 7 vol % plagioclase). Combined with the density of the mineral, the Fe–Ti oxide-rich globules are estimated to contain 43 wt% Cpx, 7 wt% Opx, 5 wt% Pl, 30 wt% Mt, and 15 wt% Ilm.

5. Sampling and analytical methods

Fourteen cumulate (rock/ore) samples in this study were collected from the Zhujiabaobao and Lanjiahuoshan open-pit mines of the Panzhihua intrusion (Lower Zone Unit II to IV; as defined by Song et al., 2013) (Fig. 2). The basalt sample ZB1443 is from an outcrop near the intrusion (Fig. 2). Sampling details including the stratigraphic locations, rock/ore types and compositions, and mineral contents are listed in Table 1.

Whole-rock major element compositions of the samples were measured with an Axios PW4400 X-ray fluorescence spectrometer (XRF) at the State Key Laboratory of Ore Deposit Geochemistry (SKLODG), Institute of Geochemistry, Chinese Academy of Sciences (IGCAS) in Guiyang, using fused Li-tetraborate glass pellets. The analytical precision, determined on the Chinese national standard GSR-3, is generally better than 5%. Detailed analytical method is the same as described in Tao et al. (2015) and Tang et al. (2017).

Compositions of the olivine, magnetite, ilmenite, clinopyroxene, orthopyroxene and plagioclase in this study were determined with a JXA8230 electron microprobe at the SKLODG, IGCAS. Analytical conditions are 25 kV accelerating voltage, 10 nA beam current and 10 μm spot diameter. Smaller beam sizes (1–5 μm) were used to measure the exsolution lamellae and smaller minerals. The peak and background counting times were 10 s and 5 s for most elements, except for 8 s (Na) and 4 s (K). The data were calibrated with natural mineral standards: For olivine: pyrope (for Ti and Cr), olivine (for Ni, Fe, Si, and Mg), plagioclase (for Na and Ca), diopside (for Al) and almandine (for Mn); For clinopyroxene and orthopyroxene: plagioclase (for K), olivine (for Ni); chrome-diopside (for Fe, Si, Mg, Na, and Ca), pyrope (for Ti and Cr), diopside (for Al), and almandine (for Mn); Magnetite and ilmenite: olivine (for Ni), magnetite (for Fe), benitoite (for Ti), vanadium (for V),

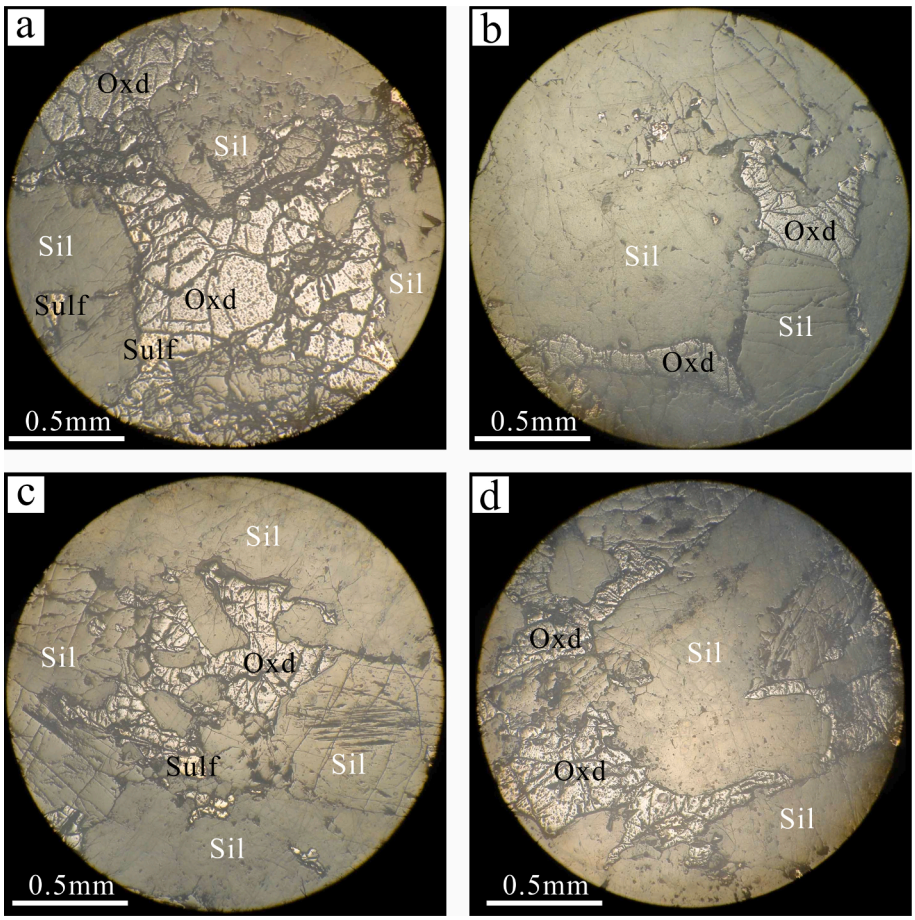

Fig. 4. Reflected-light photomicrographs of ores and Fe–Ti oxide gabbro from the Panzhihua intrusion (Lower Zone). The photos show interstitial Fe–Ti oxides among silicate mineral grains. Abbreviations: Oxd-Fe–Ti oxide; Sil-Silicate mineral; Sulf-sulfide.

pyrope (for Si and Ca), chromite (for Al and Mg), johannsenite (for Mn); For the exsolution lamellae phase: plagioclase (for K, Si, Na, Al, and Ca), olivine (for Ni), pyrope (for Fe, Cr, and Mg), kaersutite (for Ti), apatite (for P), and almandine (for Mn). The detection limits for these elements are 0.01 wt%, and the analytical uncertainty was within ± 2% of the accepted values.

6. Result

6.1. Whole-rock major elements

The whole-rock chemical compositions of the samples are given in Table 1. Compiling also the data from Zhou et al. (2005), major oxide content variations of the Panzhihua intrusion are illustrated in Fig. 10. Our data are consistent with the data from Zhou et al. (2005). Our samples are limited to the Lower Zone rocks, which are lack of the evolved ones (featured with low content in MgO, but high in SiO_2, Al_2O_3, Na_2O and K_2O). Both our data and the published ones (Zhou et al., 2005) show two clear geochemical variation trends for the ore-barren rocks and ores. The two trends intersect at the highest MgO (~10 wt%). The ore-barren rocks have <20 wt% $Fe_2O_3^T$, >35 wt% SiO_2, >10 wt% Al_2O_3, and >1.5 wt% Na_2O; whilst the ores have >20 wt% $Fe_2O_3^T$, <35 wt% SiO_2, <10 wt% Al_2O_3, and < 1.5 wt% Na_2O (Fig. 10; Table 1). The different geochemical trends for the ores and ore-barren rocks suggest that geochemical compositions of the former are controlled by Fe–Ti oxide accumulation, while those of the latter are controlled by the magma evolution. The ores can be seen as a mixture of silicate cumulate and Fe–Ti oxides. The FeO-TiO_2 correlation (Fig. 10d) shows that titanomagnetite and ilmenite in the ores occur in ratios of ~2:1 to ~1:1.

The basalt sample ZB1443 has relatively low MgO (5.58 wt%) and high $Fe_2O_3^T$ (16.17 wt%), suggesting its possible derivation from an evolved magma or with magma immiscibility in deep for its higher $Fe_2O_3^T$. The chemical compositions fall on the ore-barren rock trend (Fig. 10), suggesting a close magmatic link with the Panzhihua intrusion.

6.2. Olivine compositions

EPMA data of olivine from the intrusion are listed in Table 2. There is major compositional difference between the olivine rim and olivine primocryst (Table 2 and Fig. 11). The olivine primocrysts have lower Fo values (65.2–71.2, avg. 68.5) than those of the olivine rims (72.2–81.9, avg. 77.5). This reflects different geochemical compositions of their respective equilibrated melts, which can be used to constrain the parental magma composition of the intrusion.

6.3. Compositions of Fe–Ti oxide-rich globules

Compositions of magnetite, ilmenite, clinopyroxene, orthopyroxene, and plagioclase for Fe–Ti oxide-rich globules are listed in Table 3. Based on the mineral contents, the Fe–Ti oxide-rich globules are estimated to contain ~38 wt% FeO (Table 3), representing the immiscible Fe-rich melt segregated from the magma. Liu et al. (2014) had estimated the composition of the solid inclusions from the Baima intrusion to have >60 wt% FeO^T, representing the trapped liquids of immiscible Fe–rich melts, indicating that the trapped melts were extremely Fe–Ti-enriched. The estimated FeO content of immiscible Fe–rich melts from the Fe–Ti

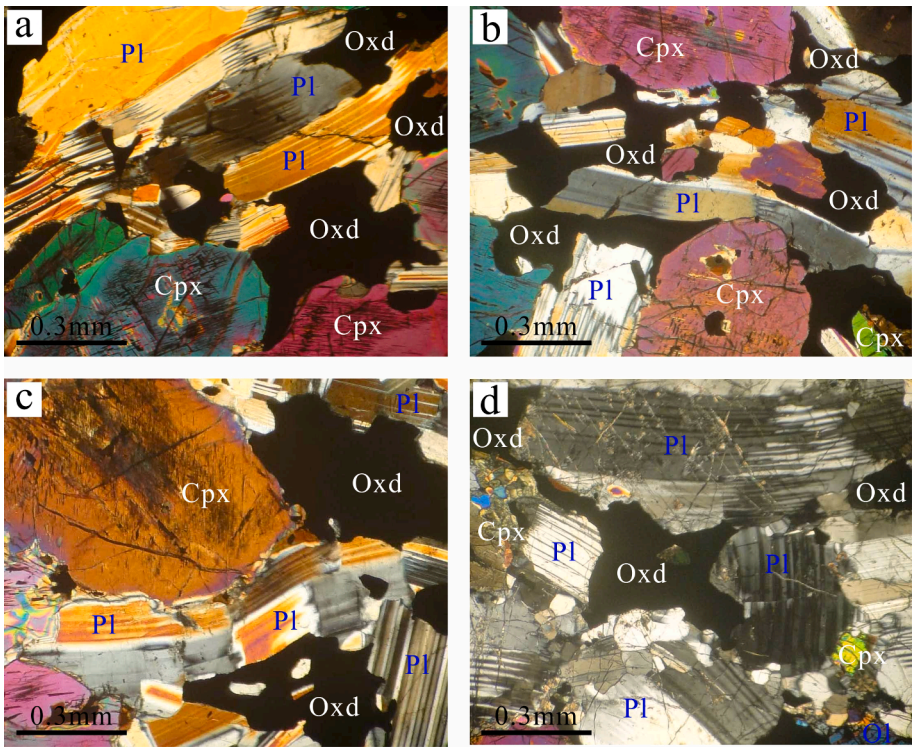

Fig. 5. Photomicrographs of Fe–Ti oxide-bearing gabbro from the Panzhihua intrusion (Lower Zone), showing kinked plagioclase (crossed polar). The rock consists of clinopyroxene, plagioclase, minor olivine, and interstitial Fe–Ti oxides. Abbreviations as in Fig. 3.

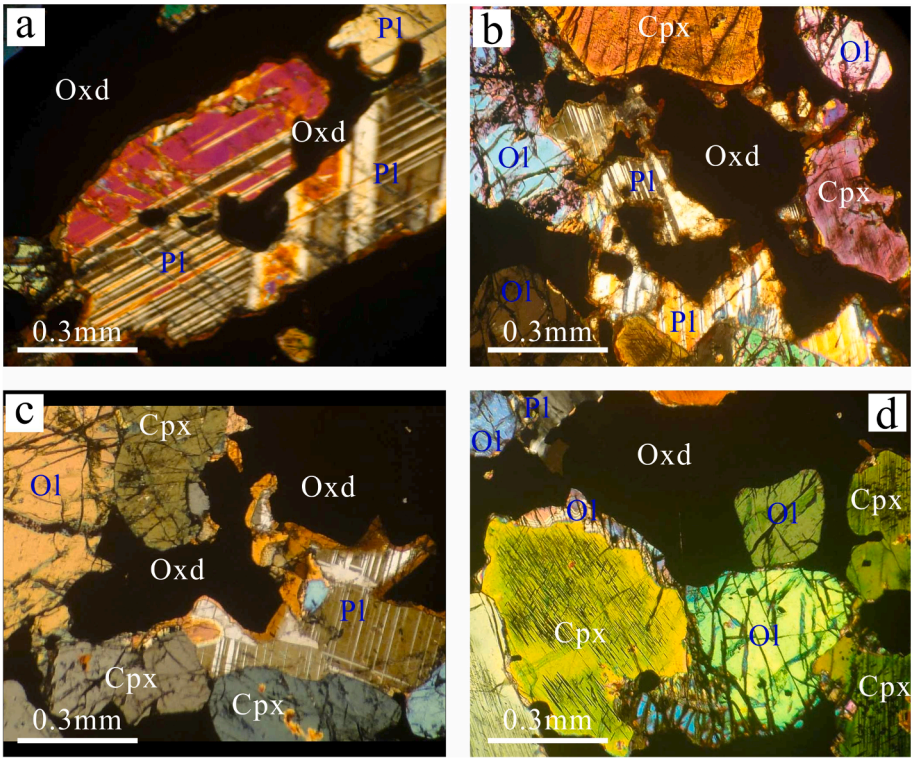

Fig. 6. Photomicrographs of the massive ores and Fe–Ti oxide-bearing gabbro from the Panzhihua intrusion (Lower Zone), showing partially-dissolved silicate primocrysts (crossed polar): (a) dissolution extending to inner crystal of euhedral primocryst plagioclase, with the eroded embayment filled with Fe–Ti oxides; (b, c) primocryst plagioclase dissolved and the embayment filled with Fe–Ti oxides; (d) euhedral Cpx, Ol and Pl primocrysts surrounded by Fe–Ti oxides. Primocryst Pl and Cpx partially dissolved with monocrystalline olivine rims. Abbreviations as in Fig. 3.

oxide-rich globules in the Panzhihua intrusion in this study is lower than that of the Fe–rich melts from the Baima intrusion reported in Liu et al. (2014), but higher than that of immiscible Fe-rich melt (26.91 wt% FeO^T, obtained by melt inclusions) from the Xijie intrusion (Panxi region) (Wang and Zhou, 2013). Compared with similar Fe–Ti oxide-rich globules from the Khungtukun intrusion (Siberian Trap) (15–22 wt% FeO^T; Kamenetsky et al., 2013), the globules from the Panzhihua intrusion have relatively high FeO contents.

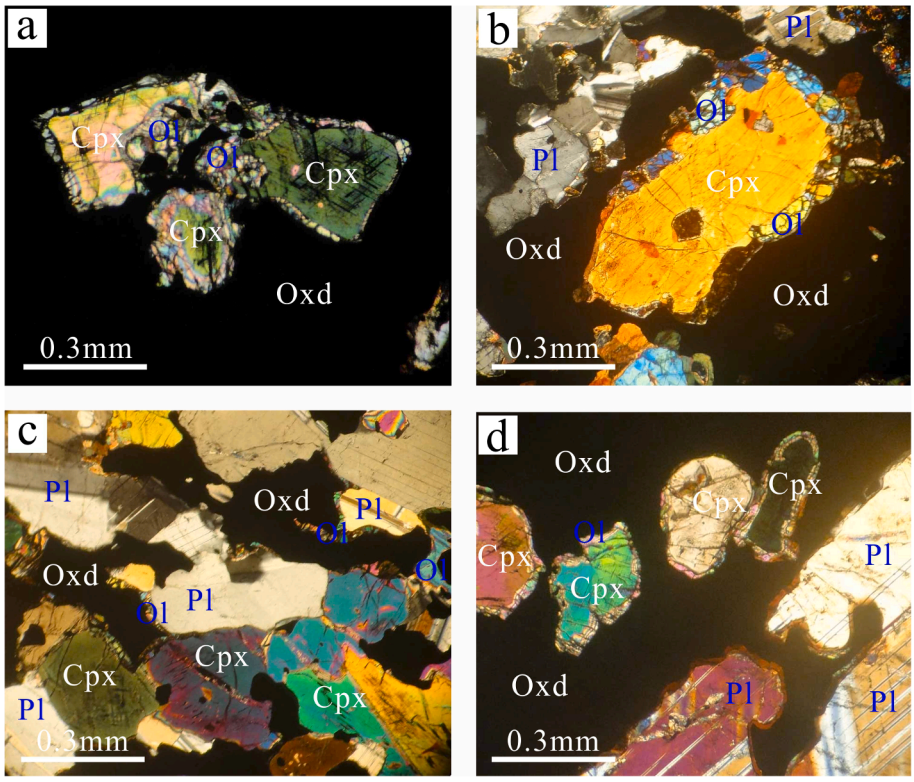

Fig. 7. Photomicrographs of the massive ores and Fe–Ti oxide-bearing gabbro from the Panzhihua Lower Zone, showing partial dissolution texture of olivine rims (crossed polar): (a, b) Cpx primocryst with Ol growth rim surrounded by Fe–Ti oxides in massive ore; (c) interstitial Fe–Ti oxides among Pl and Cpx primocrysts (with polycrystalline Ol growth rim) in Fe–Ti oxide-bearing gabbro; (d) Cpx primocryst (with monocrystalline Ol growth rim) surrounded by Fe–Ti oxides in massive ore. Abbreviations as in Fig. 3.

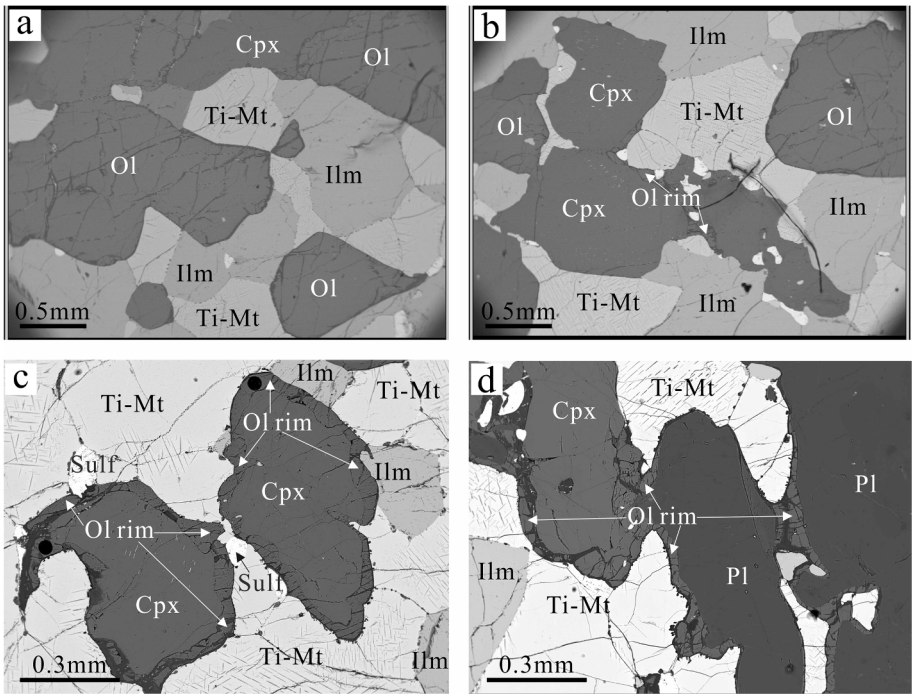

Fig. 8. Back-scattered electron images of the ores and Fe–Ti oxide bearing-gabbro from the Panzhihua Lower Zone, showing olivine primocryst and growth rim: (a, b) euhedral Ol primocryst in ores; (c, d) olivine growth rims on Cpx or Pl primocrysts. Abbreviations: Ti-Mt-titanomagnetite; Ilm-ilmenite; Sulf-sulfide; Pl-plagioclase; Cpx-clinopyroxene; Ol-olivine.

7. Discussion

7.1. Ore textures as evidence of liquid immiscibility at Panzhihua

Fe–Ti oxides occur as interstitials among silicate minerals in the ores (Figs. 4 and 6). Formation of such a texture has been conventionally proposed to be the interstitial growth from intercumulus melt within the crystal mush, coupled with convective magma circulation within the intercumulus pore space (to allow continuous interactions with the parental magma). This is followed by the squeezing out of residual

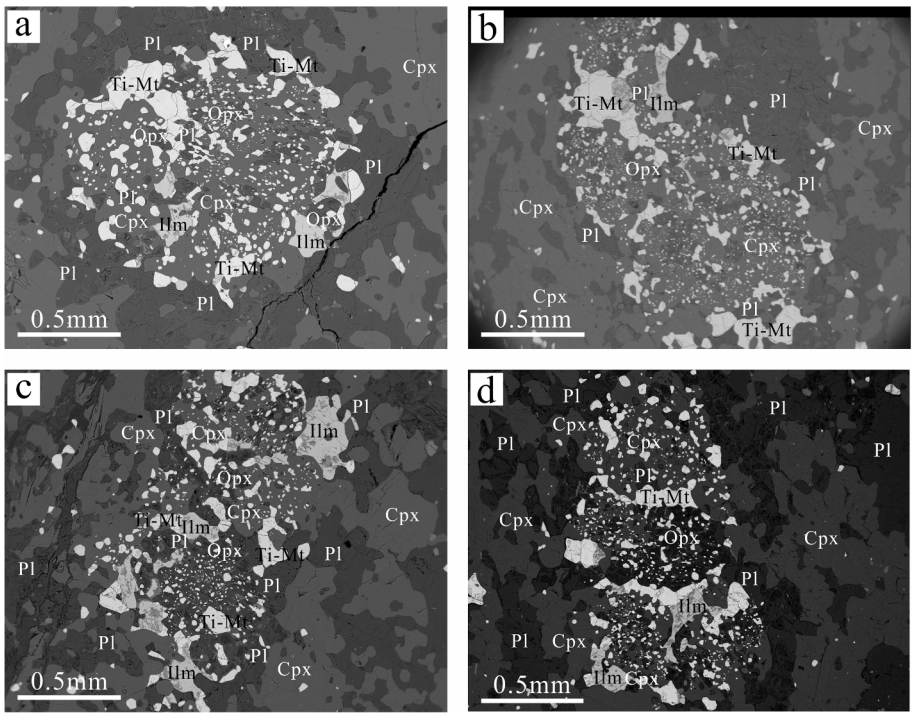

Fig. 9. Back-scattered electron images of Fe–Ti oxide-rich globules in the ore-barren gabbro (sample PZH1, Panzhihua Lower Zone). The globules are 1 ~ 2 mm large and contain aggregates of Fe–Ti oxides and silicate (Cpx, Opx and Pl) minerals. Abbreviations: Ti-Mt-titanomagnetite; Ilm-ilmenite; Cpx-clinopyroxene; Pl-plagioclase; Opx-Orthopyroxene.

Table 1
Stratigraphic position, major element compositions (wt.%) and estimated modal mineralogy of the analysed samples from the Panzhihua intrusion, SW China.

Ore segments	Lanjiahuoshan			Zhujiabaobao											
Lithological Zone	Lower Zone			Lower Zone											
Sample	LJ 1300	LJ 1303	LJ 1304	PZH 1	PZH 6	PZH 7	PZH 10	PZH 11	PZH 12	PZH 14	PZH 16	PZH 18	PZH 19	PZH 1334	ZB 1443
Meters above base of the Lower Zone	5	20	25	120	115	110	105	100	95	90	80	70	55	50	–
Rock name/Ore type	Mass ore	Mass ore	Mass ore	Gb	Net ore	Gb	Diss ore	Mass ore	Mass ore	Diss ore	Mass ore	Gb	Net ore	Net ore	Basalt
SiO_2	9.09	15.02	13.85	43.39	35.06	44.38	37.97	17.06	15.66	38.79	15.39	41.11	34.74	36.22	45.91
TiO_2	13.50	12.11	12.54	2.35	9.64	2.51	5.29	16.93	13.57	6.69	19.09	5.70	8.08	5.18	3.57
Al_2O_3	5.81	6.81	8.11	12.97	9.86	11.13	11.02	5.33	4.78	12.19	2.83	12.24	7.60	14.89	12.34
$(Fe_2O_3)^T$	60.53	53.80	54.00	14.95	24.73	14.95	24.10	47.51	48.33	20.02	45.33	17.62	26.67	24.01	16.17
MnO	0.34	0.31	0.30	0.18	0.23	0.19	0.21	0.26	0.30	0.21	0.37	0.19	0.28	0.17	0.22
MgO	4.66	5.63	4.78	10.23	8.00	9.68	7.20	6.57	6.62	6.93	9.47	6.90	8.54	5.78	5.58
CaO	2.83	4.86	4.05	10.97	10.29	14.14	11.86	6.51	5.51	11.72	4.18	13.37	11.15	10.16	8.12
Na_2O	0.04	0.06	0.07	1.37	1.45	1.95	1.67	0.27	0.29	2.78	0.19	1.83	0.95	2.16	4.31
K_2O	0.06	0.09	0.06	0.14	0.09	0.08	0.09	0.03	0.07	0.15	0.04	0.11	0.06	0.21	0.21
P_2O_5	0.03	0.01	0.01	0.25	0.05	0.18	0.04	0.04	0.02	0.07	0.02	0.06	0.03	0.04	0.58
L.O.I	1.16	0.95	0.75	2.23	0.23	0.81	0.21	0.07	1.65	0.10	0.87	1.24	1.21	0.67	2.76
Total	98.07	99.64	98.51	99.03	99.63	100.0	99.66	100.58	96.80	99.64	97.78	100.36	99.31	99.49	99.77
Olivine	–	2	–	–	5	–	5	5	7	5	5	–	5	15	–
Clinopyroxene	5	25	25	55	45	53	45	20	20	30	30	55	55	20	–
Plagioclase	25	13	10	35	20	40	30	10	13	50	5	35	15	40	–
Fe–Ti oxide	70	60	65	10	30	7	20	65	60	15	60	10	25	25	–

The mineral modal proportions were estimated visually under microscope. All the samples are generally unmetamorphosed and fresh, few samples have amphibole which is thought to be formed by alteration of clinopyroxene in late-stage of accumulation and thus not counted as primocryst. Minor minerals such as apatite are not counted in the estimation. The estimation takes only the main primocryst minerals olivine, clinopyroxene, plagioclase, and Fe–Ti oxide as 100 wt%. Fe–Ti oxide mainly consisted of Ti-Magnetite and Ilmenite. Abbreviations: Gb-gabbro; Mass ore-massive ore; Net ore-net-textured ore; Diss ore-disseminated ore.

intercumulus melt and porosity elimination (Kerr and Tait, 1985; Barnes et al., 2016).

The interstitial/matrix Fe–Ti oxides in the ores have been reported at Panzhihua and other layered intrusions in the Panxi region, and were interpreted as evidence of crystallization of Fe–Ti oxides from Fe-rich melt (e.g., Zhou et al., 2005, 2013; Dong et al., 2013; Wang and Zhou 2013; Wang et al., 2018b). However, this hypothesis is in dispute due to the shortcomings in an alleged idea of Fe–Ti-rich liquid immiscibility.

Bent plagioclase in the ores (Fig. 5) may be consistant with the origin of interstitial oxides from immiscible liquids. Plagioclase bending is a kind of crystal lattice distortion caused by uniaxial stress, which may have led by crystal mush compaction (Meurer and Boudreau 1998;

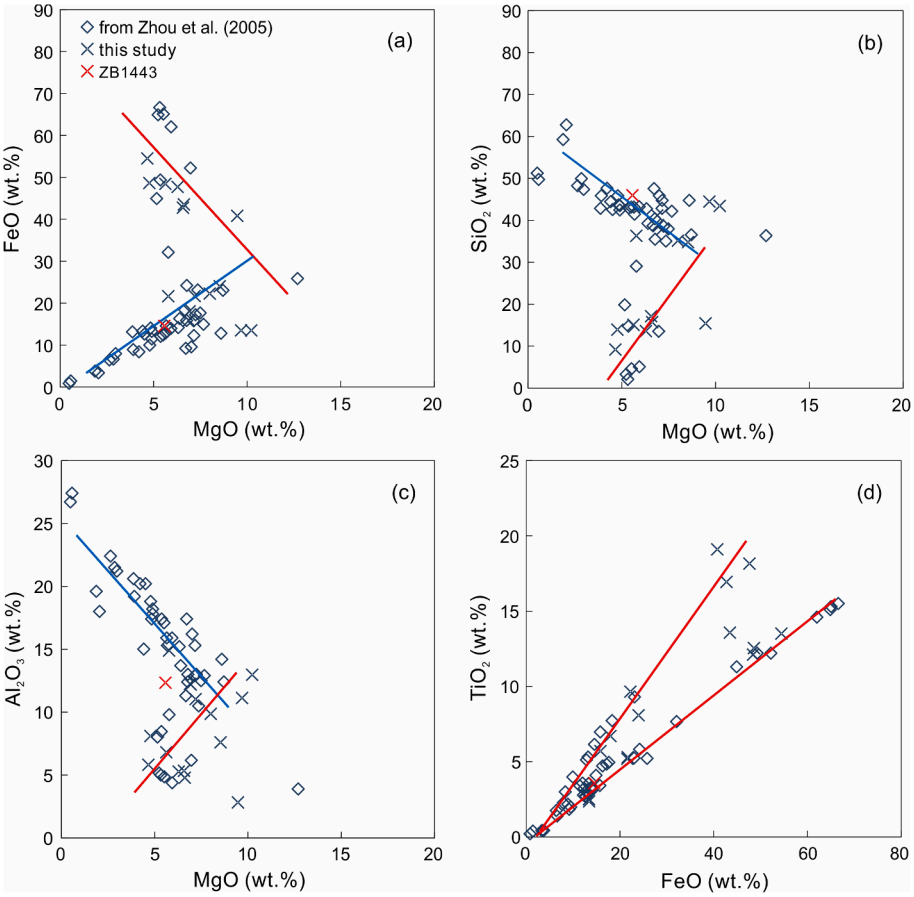

Fig. 10. Binary plots (a) FeO vs. MgO, (b) SiO_2 vs. MgO, (c) Al_2O_3 vs. MgO, and (d) TiO_2 vs. FeO of the ore-barren rocks and ores from the Panzhihua intrusion, showing the variations in major oxide concentrations.

Philpotts AR and Philpotts DE, 2005; Holness et al., 2007, 2017). It is noted that the plagioclase bent in the ores always protrude to interstitial oxide as if free surface, showing that the place of the interstitial oxide is filled with liquid in time of plagioclase bending. The oxides should be crystallized from interstitial liquid among surrounded primocrysts, and it has been verified by Fe isotopic compositions (Cao et al., 2019). This suggested that the accumulation of Fe–Ti oxides at Panzhihua cannot be explained by simple crystal fractionation associated with mineral sorting of Fe–Ti oxides. An alternative model is segregation of an immiscible Fe-rich liquid, which was then percolated to the crystal-mush zone and squeezed out the existing interstitial residual silicate melt. The Fe–Ti oxides then crystallized as interstitials among primocryst silicate minerals. Given that all the interstice are completely filled with Fe–Ti oxides, immiscible Fe-rich liquid should be replenished again and again while residual liquid squeezed out in time.

Partial plagioclase dissolution (Fig. 6) and the infill of Fe–Ti oxides in the corroded plagioclase embayment suggest that Fe–Ti oxides were crystallized after plagioclase (Zhou et al., 2005). Plagioclase primocryst dissolution may be formed by pressure drop during rapid magma ascent or magma replenishment, due to higher temperature and possible changes in melt composition (Nelson and Montana, 1992; Viccaro et al., 2010). Considering the embayments of partially-dissolved plagioclase in the Panzhihua intrusion are filled with Fe–Ti oxides, we suggest that the dissolved plagioclase was in disequilibrium with the surrounding melt before the Fe–Ti oxides crystallized, the original interstitial melt was replaced by a Fe-rich liquid.

Olivine rims had been reported widely in layered intrusions. Holness et al. (2011) had presented a detailed discussion of olivine rims in the Skaergaard Intrusion. Based on micro-structures of conjugate pairs of late-stage interstitial intergrowths (melanogranophyres and olivine rims & Fe–Ti oxide intergrowths), Holness et al. (2011) considered that liquid immiscibility took place within the crystal mush, and olivine rim was crystallized in a late stage associated with Fe–Ti oxides crystallization in a system which dominated by the Fe-rich melt (due to the removal of exsolved Si-rich droplets).

Olivine rims were observed in Fe–Ti oxide ores in the Panxi region, for instance, in the Panzhihia, Baima, and Hongge intrusions (Xing et al., 2012; Liu et al., 2016). Olivines rims commonly surround silicate primocryst grains and isolating oxide, as shown in Figs. 7 and 8. It is suggested that the late-stage liquid was likely rich in Fe and Mg, but poor in Si, Al, and Na, consistent with Fe-rich liquid derived from immiscibility. Unlike the Skaergaard Intrusion, no melanogranophyres was observed in the late-stage interstitial intergrowths at Panzhihua, and we propose that the unmixed Fe-rich liquids in the magma chamber may have percolated downward to the crystal-mush zone due to gravity, and replaced the previous interstitial melts. The interstitial space would therefore be filled with the unmixed Fe-rich liquid. Due to this sudden change in chemical conditions, primocryst plagioclases and clinopyroxenes would be resolved via disequilibration with the surrounding Fe-rich liquid, and then crystallizing the Fe–Ti oxides and olivine rim.

Apart from olivine rims, amphibole rims were observed in layered intrusion in the Panxi region. Many authors have described the amphibole rims in the ores from the Panzhihua, Baima and Hongge intrusion (Zhou et al., 2005; Xing et al., 2012; Wang and Zhou, 2013; Liu et al., 2014; Wang et al., 2020). Brown hornblende (Hbl) rimmed around plagioclase, clinopyroxene and separate the Fe–Ti oxides in massive and net-textured Fe–Ti oxide ores in the Lower Zone of the Panzhihua intrusion. Experiment studies show that amphibole coexisting with the mafic melt stably is only in the very late magmatic stages when the system is highly volatile rich as well as at relatively low temperatures

Table 2
Chemical compositions of olivine from the Panzhihua intrusion (wt.%).

Sample	Rock/Ore type	Ol type	SiO_2	MgO	FeO	MnO	CaO	NiO	Total	Fo
LJ1300-10	Ol-gb/Mass Ore	rim	38.94	39.47	20.44	0.35	0.14	0.13	99.47	77.2
LJ1304-3	Ol-gb/Mass Ore	rim	38.67	38.22	22.37	0.39	0.12	0.12	99.89	75.0
LJ1304-7		rim	38.27	37.96	22.86	0.37	0.17	0.09	99.72	74.4
LJ1304-12		rim	38.34	39.16	21.32	0.43	0.12	0.23	99.60	76.2
PZH11-1	Ol-gb/Net Ore	rim	39.35	41.35	18.47	0.37	0.08	0.18	99.80	79.6
PZH11-2		rim	39.53	40.04	19.74	0.33	0.14	0.12	99.90	78.1
PZH11-3		rim	40.30	42.57	16.48	0.26	0.12	0.09	99.82	81.9
PZH11-4		rim	38.73	40.24	19.82	0.43	0.17	0.14	99.53	78.0
PZH11-5		rim	39.19	40.67	19.31	0.33	0.13	0.03	99.66	78.7
PZH11-7		rim	39.19	40.19	19.59	0.40	0.21	0.11	99.69	78.2
PZH11-8		rim	39.00	39.85	20.36	0.33	0.15	0.04	99.73	77.4
PZH11-9		rim	39.17	40.96	19.09	0.34	0.12	0.10	99.78	79.0
PZH11-11		rim	39.33	41.43	17.97	0.33	0.13	0.19	99.38	80.1
PZH12-1	Ol-gb/Net Ore	rim	38.71	39.57	20.85	0.38	0.07	0.15	99.73	76.9
PZH12-2		rim	38.92	39.76	20.28	0.40	0.17	0.09	99.62	77.4
PZH12-3		rim	37.98	39.74	21.28	0.39	0.15	0.14	99.68	76.6
PZH12-4		rim	38.27	40.89	19.73	0.40	0.11	0.19	99.59	78.4
PZH12-6		rim	38.83	40.29	19.86	0.44	0.13	0.08	99.63	78.0
PZH12-8		rim	37.56	37.79	23.34	0.50	0.17	0.18	99.54	73.9
PZH12-18		rim	38.64	40.47	20.01	0.34	0.11	0.15	99.72	78.0
PZH12-20		rim	37.96	39.66	20.84	0.47	0.21	0.17	99.31	76.8
PZH12-22		rim	38.20	40.16	20.88	0.33	0.09	0.16	99.82	77.2
PZH12-24		rim	38.86	39.84	20.25	0.40	0.18	0.14	99.67	77.5
PZH12-26		rim	38.30	39.02	21.94	0.40	0.19	0.05	99.90	75.7
average										77.5
PZH16-2	Ol-gb/Net Ore	primocryst	38.68	33.52	26.95	0.50	0.11	0.09	99.85	68.5
PZH16-3-1		primocryst	38.66	32.76	27.64	0.52	0.12	0.11	99.81	67.5
PZH16-3-21		primocryst	39.25	34.97	24.94	0.54	0.15	0.14	99.99	71.0
PZH16-3-22		primocryst	38.60	33.76	26.93	0.51	0.10	0.09	99.99	68.7
PZH16-4-2		primocryst	38.55	33.70	26.98	0.52	0.08	0.11	99.94	68.6
PZH16-4-3		primocryst	38.55	33.76	27.04	0.48	0.06	0.07	99.96	68.6
PZH16-5-1		primocryst	38.84	33.20	27.54	0.50	0.10	0.05	100.23	68.2
PZH16-5-8		primocryst	38.88	33.56	26.48	0.56	0.17	0.13	99.78	68.9
PZH16-6-5		primocryst	38.75	33.37	27.25	0.50	0.08	0.04	99.99	68.2
PZH16-6-7		primocryst	39.04	34.83	25.34	0.48	0.12	0.07	99.88	70.6
PZH16-6-11		primocryst	38.78	33.08	27.42	0.48	0.13	0.06	99.95	67.9
PZH16-6-12		primocryst	39.14	35.16	24.85	0.53	0.05	0.08	99.81	71.2
PZH16-6-16		primocryst	38.28	32.86	27.93	0.61	0.11	0.12	99.91	67.2
PZH16-6-17		primocryst	38.96	34.08	26.10	0.50	0.15	0.06	99.85	69.5
PZH16-6-20		primocryst	39.26	35.50	24.50	0.45	0.14	0.03	99.88	71.7
PZH16-7-1		primocryst	38.34	33.16	27.40	0.60	0.14	0.14	99.78	67.9
PZH19-3-1	Ol-gb/Diss Ore	primocryst	37.68	31.98	29.46	0.59	0.13	0.07	99.91	65.5
PZH19-4-2		primocryst	37.79	31.73	29.49	0.66	0.14	0.06	99.87	65.2
PZH19-4-3		primocryst	37.84	32.59	28.42	0.61	0.16	0.15	99.77	66.7
average										68.5

Abbreviations: Ol-olivine; Ol-gb-olivine gabbro; Mass Ore-massive ore (Fe–Ti oxides > 60 vol%); Net Ore-net-textured ore (Fe–Ti oxides = 20–60 vol%); Diss Ore-disseminated ore (Fe–Ti oxides < 20 vol%).

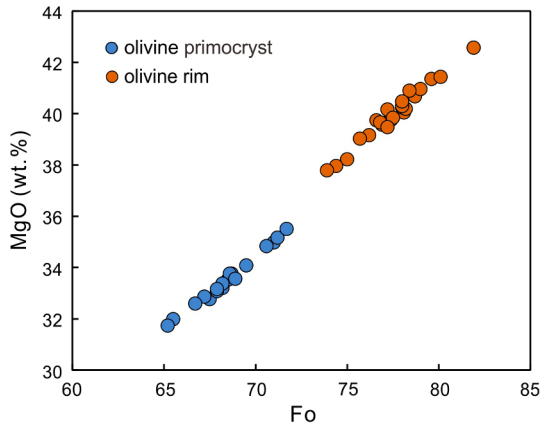

Fig. 11. Binary plots MgO-Fo of the olivine grains and growth rims from the Panzhihua intrusion.

(<1000 °C) (Botcharnikov et al., 2008; Fiorentini et al., 2008; Wang et al., 2020). The occurrence of amphibole rims in the Fe–Ti oxide ores indicate that the late-stage liquid should be volatile-rich, which may have triggered immiscibility as proposed in previous studies (e.g., Zhou et al., 2005; Wang and Zhou, 2013; Liu et al., 2014). The H_2O content could be enriched during crystallization or introduced into the melts through magma-wallrock interaction during or after the magma emplacement (Zhou et al., 2005; Wang and Zhou, 2013; Liao et al., 2016).

7.2. Parental magma of the Panzhihua intrusion and Fe–Ti-oxide ore-forming liquids

Olivine primocrysts and rims from Panzhihua have Fo contents of 65.2 to 71.2 (avg. 68.5) and 72.2 to 81.9 (avg. 77.5), respectively, which are distinctly lower than those of olivine phenocrysts in the Emeishan picrite (Zhang et al., 2006; Li et al., 2012; Putirka et al., 2018; Yu et al., 2020) and the sulfide ore-bearing intrusion. This indicates that the parental magmas at Panzhihua are more evolved than those of the sulfide ore-bearing intrusion and Emeishan picrite.

By appropriating Kd(Fe–Mg) oliv-liq = 0.3 (Roeder and Emslie, 1970; Matzen et al., 2011), MgO and FeO contents of the parental

Table 3
Composition of the minerals in Fe–Ti oxide-rich globule in sample PZH1 (wt.%) and the estimated composition of the Fe–Ti oxide-rich globule.

	SiO_2	TiO_2	Al_2O_3	FeO	MnO	MgO	CaO	Na_2O	V_2O_5	Total
Cpx1	51.65	0.35	1.79	7.05	0.24	14.34	21.44	0.35	–	97.21
Cpx2	52.48	0.48	1.68	7.00	0.25	14.39	21.83	0.30	–	98.41
Cpx3	52.85	0.42	1.85	7.93	0.25	14.46	21.29	0.33	–	99.38
Cpx4	51.88	0.26	1.46	6.94	0.26	14.50	21.96	0.37	–	97.63
Cpx5	53.87	0.41	1.71	7.09	0.24	15.40	22.08	0.36	–	101.16
Cpx6	53.22	0.44	1.69	6.98	0.23	14.85	21.96	0.32	–	99.69
Cpx7	53.36	0.37	1.61	7.13	0.19	15.02	22.19	0.40	–	100.27
Cpx8	52.05	0.36	1.70	6.99	0.25	14.53	21.89	0.25	–	98.02
Cpx9	53.45	0.36	1.66	7.39	0.26	14.78	21.59	0.30	–	99.79
Cpx10	53.23	0.41	1.81	7.52	0.23	14.57	21.85	0.37	–	99.99
Cpx11	52.75	0.32	1.70	7.43	0.27	14.83	21.57	0.34	–	99.21
Cpx12	53.85	0.60	1.81	7.50	0.27	15.06	21.54	0.38	–	101.01
Cpx13	53.53	0.42	1.71	7.86	0.28	15.01	21.40	0.39	–	100.6
Cpx14	50.77	0.49	2.33	7.61	0.31	14.79	21.74	0.40	–	98.44
Cpx15	52.25	0.35	1.96	6.85	0.27	15.16	22.32	0.38	–	99.54
Cpx16	52.09	0.49	2.12	7.44	0.25	15.27	21.86	0.42	–	99.94
Cpx17	51.93	0.38	2.14	7.29	0.28	14.94	21.81	0.41	–	99.18
Cpx18	51.81	0.50	2.44	7.64	0.25	14.79	21.82	0.37	–	99.62
Cpx19	52.24	0.42	1.96	7.47	0.25	15.32	21.71	0.39	–	99.76
Cpx20	52.06	0.44	1.99	7.78	0.27	15.37	21.77	0.42	–	100.10
Cpx21	51.93	0.39	1.90	6.77	0.25	15.55	22.39	0.35	–	99.53
Cpx22	51.53	0.44	2.12	7.40	0.21	15.04	21.79	0.40	–	98.93
Cpx23	52.43	0.44	2.82	7.64	0.28	14.14	22.05	0.37	–	100.17
Average	52.49	0.41	1.91	7.33	0.25	14.87	21.82	0.36	–	99.44
Opx1	44.20	0.14	12.86	18.74	0.18	22.24	1.35	0.11	–	99.82
Opx2	42.53	0.05	14.01	19.22	0.16	22.80	0.87	0.09	–	99.73
Opx3	39.92	0.08	14.84	20.77	0.19	23.15	0.73	0.13	–	99.81
Opx4	44.65	0.11	12.74	18.85	0.24	21.47	1.48	0.12	–	99.66
Average	42.83	0.10	13.61	19.40	0.19	22.42	1.11	0.11	–	99.77
Pl1	52.38	0.01	29.07	0.47	0.01	0.03	9.64	4.61	–	96.22
Pl2	51.98	–	29.81	0.39	0.01	0.03	10.18	4.16	–	96.56
Pl3	52.71	0.03	30.19	0.56	0.01	–	10.23	4.37	–	98.10
Average	52.36	0.01	29.69	0.47	0.01	0.02	10.02	4.38	–	96.96
Mt1	0.53	4.88	2.99	90.33	0.16	0.22	0.06	–	0.61	99.78
Mt2	0.42	10.65	0.77	87.14	0.10	0.17	0.16	–	0.68	100.09
Mt3	0.37	10.05	2.71	85.81	0.02	0.22	0.30	–	0.73	100.21
Mt4	0.54	4.40	2.02	91.82	0.10	0.28	–	–	0.64	99.80
Mt5	0.41	3.96	3.29	89.88	0.21	0.76	0.21	–	0.79	99.51
Mt6	0.52	3.82	3.40	89.32	0.27	0.83	0.06	–	0.77	98.99
Mt7	0.61	4.51	3.36	89.33	0.19	0.44	0.24	–	0.65	99.33
Average	0.49	6.04	2.65	89.09	0.15	0.42	0.15		0.70	99.69
Ilm1	–	44.66	0.11	45.96	4.35	0.07	0.02	–	5.89	101.06
Ilm2	–	43.99	0.11	45.84	4.30	0.03	0.07	–	5.77	100.11
Ilm3	0.02	44.17	0.04	46.49	4.07	0.01	0.05	–	5.73	100.58
Ilm4	0.14	44.93	0.02	45.30	4.26	0.05	–	–	5.97	100.67
Ilm5	–	44.93	0.03	45.43	4.38	0.06	–	–	5.85	100.68
Ilm6	0.02	45.04	0.03	45.55	4.38	0.02	–	–	5.93	100.97
Average	0.03	44.62	0.06	45.76	4.29	0.04	0.02	–	5.86	101.34
Silicate phase	51.25	0.33	5.92	8.24	0.22	14.48	18.11	0.69	–	99.26
Oxide phase	0.34	18.90	1.79	74.65	1.53	0.29	0.11	–	2.42	100.24
Fe–Ti oxide Rich globule as a whole	28.34	8.69	4.06	38.12	0.81	8.10	10.01	0.38	1.09	99.70

Mineral contents of the Fe–Ti oxide-rich globule are estimated to contain 43 wt% Cpx, 7 wt% Opx, 5 wt% Pl, 30 wt% Mt, and 15 wt% Ilm. Abbreviations: Cpx-clinopyroxene; Opx-Orthopyroxene; Pl-plagioclase; Mt-magnetite; Ilm-ilmenite.

magma is likely located in line of Fo = 68.5. As shown in Fig. 12, the compositions of the olivine primocryst match well with the sample ZB1443 basalt ($Fe_2O_3^T$ = ~16 wt%). It is reasonable to assume that the latter mimics that of the Panzhihua parental magma, which was equilibrated with the olivine primocrysts in the ores.

Late-stage olivine rims are associated with the immiscible Fe-rich liquid (now represented by Fe–Ti oxide-rich globules), but the olivine rims do not match well with the composition of the globules. It is reasonable to assume that Fe–Ti oxides would crystallize before other silicate minerals and decrease the FeO content of the Fe-rich liquids. The olivine rims should be equilibrated with residual liquids after Fe–Ti oxide crystallization. Based on the estimation by geometric proportion simulated calculation (Fig. 12), Fe-rich liquids would evolve to crystallize olivine rims after ~33% Fe–Ti oxide crystallization. Therefore, we assume that the Fe–Ti oxide-rich globules (Table 3) in PZH1 are equivalent to the Fe–Ti oxide-forming melt, whereas the basalt sample ZB1443 is equivalent to the parental magma of the intrusion.

7.3. Implications for the origin of the Fe–Ti oxide ores

Fe-rich globules are estimated as a whole, having 38 wt% FeO. The melt with such high FeO contents cannot be formed by simple magma fractionation, but can be formed by liquid immiscibility (Toplis and Carroll 1996). Fe-rich globules in sample PZH1 likely represent immiscible Fe-rich liquid droplets in the intrusion.

Ore textures suggest that the Fe–Ti oxides in the ores and Fe–Ti oxide gabbros were crystallized from interstitial melts. Partially-dissolved plagioclase and olivine rims reveal chemical disequilibrium with interstitial melts, which may have been replaced by Fe-rich liquids. The ore textures and olivine compositions record the abrupt change of liquid compositions in the ore-forming stage. All these lines of evidence agree well with an immiscible Fe-rich liquid metallogenic origin.

We therefore suggest that magma immiscibility occurred due to magma evolution and temperature drop, and then density-led liquid segregation occurred. Subsequently, the Fe-rich liquids sunk and

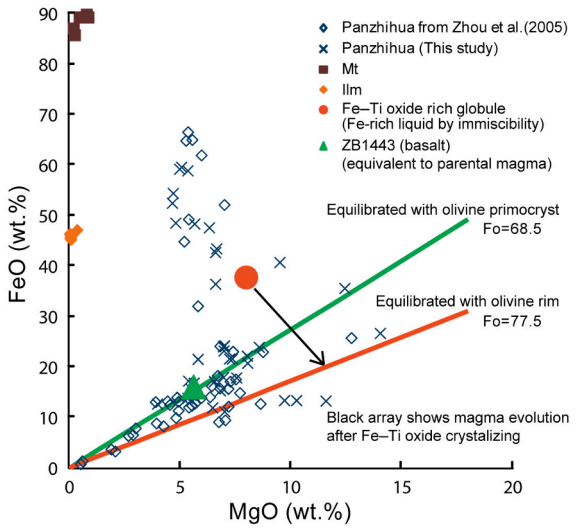

Fig. 12. Parental magma of the intrusion and immiscible liquids: constraints on olivine primocryst and rim. Green and red lines represent the liquid equilibrated with olivine primocryst (Fo = 68.5) and olivine rim (Fo = 77.5) respectively, by using KD(Fe–Mg) oliv-liq = 0.3 (Roeder and Emslie, 1970; Matzen et al., 2011). The olivine primocryst composition matches well with that of the basalt (sample ZB1443), whilst the olivine rim composition matches with that of the residual after ~33% Fe–Ti oxide crystallization from the immiscible Fe-rich liquid (represented by Fe–Ti oxide-rich globules). (For interpretation of the references to colour in this figure legend, the reader is referred to the web version of this article.)

squeezed the intersitial melts out of the crystal mush to form a Fe-rich liquid–crystal mush zone above the solidified layer in the chamber. For the Fe-rich liquids are not pure Fe–Ti oxide liquids, we propose continuous replenishment of immiscible Fe-rich liquids may have occurred to replace the residual melts after Fe–Ti oxide crystallization, until all the interstices were completely filled with Fe–Ti oxides (Fig. 13).

We propose that the parental magma of the Panzhihua intrusion was likely an evolved magma with ~16 wt% $Fe_2O_3^T$. Minerals including olivine, clinopyroxene and plagioclase may have first crystallized in the magma chamber, and accumulated to form the crystal-mush zone above the solidified layer. When the magma started to cool down, liquid immiscibility may have taken place to form a Fe-rich and a Si-rich components. The former may have compositions similar to the Fe–Ti oxide-rich globules (~38 wt% FeO) analyzed in this study.

The segregated Fe-rich droplets may have then sunk and squeezed out the original interstitial melt in the crystal mush. The compositional difference between the new Fe-rich interstitial melt and the crystal mush may have formed the partial dissolution textures of plagioclase and clinopyroxene, together with olivine growth rims. We suppose that continuous replenishment of Fe-rich liquid may have occurred to upgrade the Fe–Ti oxide ores from semi-massive/net-textured to massive ores (Fig. 13). The multiphase replenishment may also have formed the multiple ore-layers observed, as also suggested previously (Song et al., 2013).

Zhou et al. (2013) suggested that the Panzhihua Fe–Ti oxide deposit may have formed by two stages of magma immiscibility, one at depth and the other in the shallow-crustal magma chamber, and our model only covers the latter. We consider that magma immiscibility at depth may have formed the parental magma of the intrusion. We estimated that the parental magma of the intrusion has ~16 wt% FeO, and nearly all the primocryst clinopyroxene in the ores contains abundant oxide lamellae, as mentioned by Zhou et al. (2005) and Pang et al. (2009). This means that the parental magma is particularly rich in FeO. Considering the associated felsic rocks of layered intrusions in the Panxi region (Shellnutt et al., 2009; Zhong et al., 2009, 2011), magma immiscibility at depth is acceptable in our view.

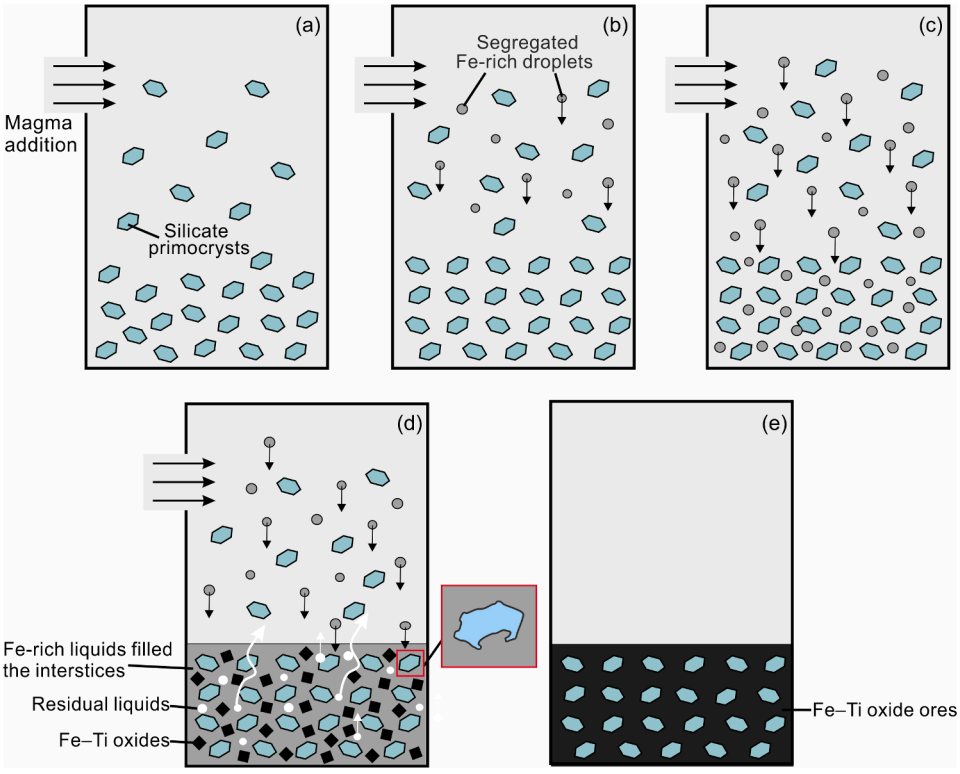

Fig. 13. Schematic illustration of the liquid immiscibility and ore-forming process in the Panzhihua intrusion. (a) Silicate primocrysts including olivine, clinopyroxene and plagioclase crystallized in the magma chamber, and accumulated to form the crystal-mush zone above the solidified layer. (b) Liquid immiscibility took place to form Fe-rich liquids due to magma evolution and temperature drop, and then density-led liquid segregation occurred. The Fe-rich liquids may have compositions similar to the Fe–Ti oxide-rich globules (~38 wt% FeO) analyzed in this study. (c) The segregated Fe-rich droplets percolated downward to the crystal-mush zone due to gravity, and squeezed out the original interstitial melts. (d) The Fe-rich liquids sunk and squeezed the interstitial melts out of the crystal mush to form a Fe-rich liquid-crystal mush zone above the solidified layer in the chamber. Fe–Ti oxides were crystallized from the interstitial melts. For the Fe-rich liquids are not pure Fe–Ti oxide liquids, it is proposed that continuous replenishment of immiscible Fe-rich liquids occurred to replace the residual melts after Fe–Ti oxide crystallization, until all the interstices were completely filled with Fe–Ti oxides. The inset shows the primocryst silicate minerals (especially plagioclase) are dissolved via disequilibration with the surrounding Fe-rich liquids. (e) Net-textured to massive ore layer is formed by continuous replenishment of Fe-rich liquid in the crystal-mush zone above the solidified layer.

8. Conclusions

(1) Ore textures of the Fe–Ti oxide ores from Panzhihua cannot be explained by simple crystal fractionation and density-sorting of Fe–Ti oxides, but can be better interpreted by segregation of the immiscible, dense Fe-rich liquid.
(2) Fe–Ti oxide-rich globules in the Panzhihua intrusion have an average FeO content of ~38.1 wt%, and likely represent the solidified immiscible Fe-rich liquid in the Panzhihua intrusion.
(3) The ore layers may have formed by density-driven sinking and concentration of immiscible Fe-rich liquids, which squeezed out the original silicate-rich residual melts from the crystal mush, forming the Fe–Ti oxide ore layers.

CRediT authorship contribution statement

Feng Xiong: Conceptualization, Investigation, Writing - original draft. **Yan Tao:** Supervision, Funding acquisition, Writing - review & editing. **Mingyang Liao:** Investigation, Writing - review & editing. **Yuqi Liao:** Investigation, Writing - review & editing. **Jun Ma:** Investigation, Visualization.

Declaration of Competing Interest

The authors declare that they have no known competing financial interests or personal relationships that could have appeared to influence the work reported in this paper.

Acknowledgements

We thank Drs. Christina Yan Wang, Dr. Tong Hou, and the other two anonymous reviewers for their constructive reviews. This study was supported by the Strategic Priority Research Program (B) of the Chinese Academy of Sciences (XDB18000000), National Natural Science Foundation of China (42073048, 41473051), and the High-Level Talent Initial Funding of Guizhou Institute of Technology (XJGC20190606).

Appendix A. Supplementary material

Supplementary data to this article can be found online at https://doi.org/10.1016/j.jseaes.2021.104683.

References

Bai, Z.J., Zhong, H., Hu, R.Z., Zhu, W.G., Hu, W.J., 2019. Composition of the chilled marginal rocks of the Panzhihua layered intrusion, Emeishan Large Igneous Province, SW China: implications for parental magma compositions, sulfide saturation history, and Fe–Ti oxide mineralization. J. Petrol. 60, 619–648.
Barnes, S.J., Mole, D.R., Le Vaillant, M., Campbell, M.J., Verrall, M.R., Roberts, M.P., Evans, N.J., 2016. Poikilitic textures, heteradcumulates and zoned orthopyroxenes in the ntaka ultramafic complex, Tanzania: Implications for crystallization mechanisms of oikocrysts. J. Petrol. 57 (6), 1171–1198.
Botcharnikov, R.E., Almeev, R.R., Koepke, J., Holtz, F., 2008. Phase relations and liquid lines of descent in hydrous ferrobasalt—implications for the Skaergaard intrusion and Columbia River flood basalts. J. Petrol. 49, 1687–1727.
Cao, Y.H., Wang, C.Y., Huang, F., Zhang, Z.F., 2019. Iron isotope systematics of the Panzhihua mafic layered intrusion associated with giant Fe-Ti oxide deposit in the Emeishan large igneous province, SW China. J. Geophys. Res. Solid Earth 124, 358–375.
Charlier, B., Namur, O., Toplis, M.J., Schiano, P., Cluzel, N., Higgins, M.D., Auwera, J.V., 2011. Large-scale silicate liquid immiscibility during differentiation of tholeiitic basalt to granite and the origin of the Daly gap. Geology 39, 207–210.
Charlier, B., Grove, T.L., 2012. Experiments on liquid immiscibility along tholeiitic liquid lines of descent. Contrib. Miner. Petrol. 164, 27–44.
Charlier, B., Namur, O., Grove, T.L., 2013. Compositional and kinetic controls on liquid immiscibility in ferrobasalt–rhyolite volcanic and plutonic series. Geochim. Cosmochim. Acta 113, 79–93.
Chen, L.M., Song, X.Y., Hu, R.Z., Yu, S.Y., He, H.L., Dai, Z.H., She, Y.W., Xie, W., 2017. Controls on trace-element partitioning among co-crystallizing minerals: evidence from the Panzhihua layered intrusion, SW China. Am. Mineral. 102, 1006–1020.
Dong, H., Xing, C.M., Wang, C.Y., 2013. Textures and mineral compositions of the Xinjie layered intrusion, SW China: Implications for the origin of magnetite and fractionation process of Fe-Ti-rich basaltic magmas. Geosci. Front. 4, 503–515.
Fiorentini, M.L., Beresford, S.W., Deloule, E., Hanski, E., Stone, W.E., Pearson, N.J., 2008. The role of mantle-derived volatiles in the petrogenesis of Palaeoproterozoic ferropicrites in the Pechenga Greenstone Belt, northwestern Russia: Insights from in-situ microbeam and nanobeam analysis of hydromagmatic amphibole. Earth Planet. Sci. Lett. 268, 2–14.
Fischer, L.A., Wang, M., Charlier, B., Namur, O., Roberts, R.J., Veksler, I.V., Cawthorn, R. G., Holtz, F., 2016. Immiscible iron- and silica-rich liquids in the upper zone of the bushveld complex. Earth Planet. Sci. Lett. 443, 108–117.
Holness, M.B., Anderson, A.T., Martin, V.M., MacLennan, J., Passmore, E., Schwindinger, K., 2007. Textures in partially solidified crystalline nodules: A window into the pore structure of slowly cooled mafic intrusions. J. Petrol. 48, 1243–1264.
Holness, M.B., Stripp, G., Humphreys, M.C.S., Veksler, I.V., Nielsen, T.F.D., Tegner, C., 2011. Silicate liquid immiscibility within the crystal mush: late-stage magmatic microstructures in the Skaergaard intrusion, East Greenland. J. Petrol. 52, 175–222.
Holness, M.B., Vukmanovic, Z., Mariani, E., 2017. Assessing the role of compaction in the formation of adcumulates: a microstructural perspective. J. Petrol 58 (4), 643–674.
Hou, T., Zhang, Z.C., Encarnacion, J., Santosh, M., 2012. Petrogenesis and metallogenesis of the Taihe gabbroic intrusion associated with Fe–Ti-oxide ores in the Panxi district, Emeishan Large Igneous Province, southwest China. Ore Geol. Rev. 49, 109–127.
Hou, T., Veksler, I.V., 2015. Experimental confirmation of high-temperature silicate liquid immiscibility in multicomponent ferrobasaltic systems. Am. Mineral. 100, 1304–1307.
Howarth, G.H., Prevec, S.A., Zhou, M.-F., 2013. Timing of Ti-magnetite crystallization and silicate disequilibrium in the Panzhihua mafic layered intrusion: implications for ore-forming processes. Lithos 170–171, 73–89.
Humphreys, M.C.S., 2011. Silicate liquid immiscibility within the crystal mush: evidence from Ti in plagioclase from the Skaergaard intrusion. J. Petrol. 52, 147–174.
Jakobsen, J.K., Veksler, I.V., Tegner, C., Brooks, C.K., 2005. Immiscible iron- and silica-rich melts in basalt petrogenesis documented in the Skaergaard intrusion. Geology 33, 885–888.
Jakobsen, J.K., Veksler, I.V., Tegner, C., Brooks, C.K., 2011. Crystallization of the Skaergaard intrusion from an emulsion of immiscible iron- and silica-rich liquids: evidence from melt inclusions in plagioclase. J. Petrol. 52, 345–373.
Kamenetsky, V.S., Charlier, B., Zhitova, L., Sharygin, V., Davidson, P., Fein, S., 2013. Magma-chamber-scale liquid immiscibility in the Siberian Traps represented by melt pools in native iron. Geology 41, 1091–1094.
Kerr, R.C., Tait, S.R., 1985. Convective exchange between pore fluid and an overlying reservoir of dense fluid: a post-cumulus process in layered intrusions. Earth Planet. Sci. Lett. 75, 147–156.
Li, C., Tao, Y., Qi, L., Ripley, E.M., 2012. Controls on PGE fractionation in the Emeishan picrites and basalts: constraints from integrated lithophile-siderophile elements and Sr-Nd isotopes. Geochim. Cosmochim. Acta 90, 12–32.
Li, C., Ripley, E.M., Tao, Y., 2019. Chapter X: Magmatic Ni-Cu and Pt-Pd sulfide deposits in China. Soc. Econ. Geol. Spec. Publ. 22, 483–508.
Liao, M.Y., Tao, Y., Song, X.Y., Li, Y.B., Xiong, F., 2015. Multiple magma evolution and ore-forming processes of the Hongge layered intrusion, SW China: Insights from Sr-Nd isotopes, trace elements and platinum-group elements. J. Asian Earth Sci. 113, 1082–1099.
Liao, M.Y., Tao, Y., Song, X.Y., Li, Y.B., Xiong, F., 2016. Study of oxygen fugacity during magma evolution and ore genesis in the Hongge mafic–ultramafic intrusion, the Panxi region, SW China. Acta Geochim. 35, 25–42.
Lindsley, D.H., Epler, N., 2017. Do Fe-Ti-oxide magmas exist? Probably not! Am. Mineral. 102, 2157–2169.
Liu, P.-P., Zhou, M.-F., Chen, W.T., Boone, M., Cnudde, V., 2014. Using multiphase solid inclusions to constrain the origin of the Baima Fe–Ti–(V) oxide deposit, SW China. J. Petrol. 55, 951–976.
Liu, P.-P., Zhou, M.-F., Ren, Z.Y., Wang, C.Y., Wang, K., 2016. Immiscible Fe- and Si-rich silicate melts in plagioclase from the Baima mafic intrusion (SW China): Implications for the origin of bi-modal igneous suites in large igneous provinces. J. Asian Earth Sci. 127, 211–230.
Liu, P.-P., Liang, J., Zhou, M.-F., Chen, W.T., 2020. Micro-textures and chemical compositions of metamorphic magnetite and ilmenite: Insights from the Mianhuadi mafc complex in SW China. J. Asian Earth Sci. 192, 104264.
Matzen, A.K., Baker, M.B., Beckett, J.R., Stolper, E.M., 2011. Fe–Mg partitioning between olivine and high-magnesian melts and the nature of Hawaiian parental liquids. J. Petrol. 52, 1243–1263.
Ma, Y.X., Ji, X.T., Li, J.C., Huang, M., Kan, Z.Z., 2003. Mineral Resources of the Panzhihua Region. Sichuan Science and Technology Press, Chengdu, p. 275 pp. (in Chinese).
McBirney, A.R., 2008. Comments on: 'liquid immiscibility and the evolution of basaltic magma' Journal of Petrology 48, 2187–2210. J. Petrol. 49, 2169–2170.
Meurer, W.P., Boudreau, A.E., 1998. Compaction of igneous cumulates. Part I. Whole-rock compositions as an indicator of the trapped liquid proportions in the Stillwater complex. Montana. J. Geol. 106, 281–292.
Namur, O., Charlier, B., Holness, M.B., 2012. Dual origin of Fe–Ti–P gabbros by immiscibility and fractional crystallization of evolved tholeiitic basalts in the Sept Iles layered intrusion. Lithos 154, 100–114.
Nelson, S.T., Montana, A., 1992. Sieve-textured plagioclase in volcanic rocks produced by rapid decompression. Am. Mineral. 77, 1242–1249.

Pang, K.-N., Zhou, M.-F., Lindsley, D.H., Zhao, D.G., Malpas, J., 2008. Origin of Fe–Ti Oxide ores in mafic intrusions: evidence from the panzhihua intrusion, SW China. J. Petrol. 49, 295–313.
Pang, K.-N., Li, C., Zhou, M.-F., Ripley, E.M., 2009. Mineral compositional constraints on petrogenesis and oxide ore genesis of the late Permian Panzhihua layered gabbroic intrusion, SW China. Lithos 110, 199–214.
Pang, K.-N., Zhou, M.-F., Qi, L., Chung, S.-L., Chu, C.-H., Lee, H.-Y., 2013. Petrology and geochemistry at the Lower zone-Middle zone transition of the Panzhihua intrusion, SW China: implications for differentiation and oxide ore genesis. Geosci. Front. 4, 517–533.
Philpotts, A.R., 1982. Compositions of immiscible liquids in volcanic rocks. Contrib. Miner. Petrol. 80, 201–218.
Philpotts, A.R., Doyle, C.D., 1983. Effect of magma oxidation state on the extent of silicate liquid immiscibility in a tholeiitic basalt. Am. J. Sci. 283, 967–986.
Philpotts, A.R., Philpotts, D.E., 2005. Crystal-mush compaction in the Cohassett flood-basalt flow, Hanford, Washington. J. Volcanol. Geoth. Res. 145, 192–206.
Philpotts, A.R., 2008. Comments on: Liquid immiscibility and the evolution of basaltic magma. J. Petrol. 49, 2171–2175.
Putirka, K., Tao, Y., Hari, K.R., Perfit, M.R., Jackson, M.G., Arevalo Jr., R., 2018. The mantle source of thermal plumes: Trace and minor elements in olivine and major oxides of primitive liquids (and why the olivine compositions don't matter). Am. Mineral. 103, 1253–1270.
Ripley, E.M., Severson, M.J., Hauck, S.A., 1998. Evidence for sulfide and Fe–Ti–P–rich liquid immiscibility in the Duluth complex. Minnesota. Econ. Geol. 93, 1052–1062.
Roeder, P.L., Emslie, R.F., 1970. Olivine-liquid equilibrium. Contrib. Miner. Petrol. 29, 275–289.
Shellnutt, J.G., Zhou, M.-F., Zellmer, G.F., 2009. The role of Fe–Ti oxide crystallization in the formation of A-type granitoids with implications for the Daly gap: an example from the Permian Baima igneous complex, SW China. Chem. Geol. 259, 204–217.
Song, X.Y., Zhou, M.-F., Cao, Z.M., Sun, M., Wang, Y.L., 2003. Ni–Cu–(PGE) magmatic sulfide deposits in the Yangliuping area, Permian Emeishan igneous province, SW China. Miner. Deposita 38, 831–843.
Song, X.Y., Zhou, M.-F., Tao, Y., Xiao, J.F., 2008. Controls on the metal compositions of magmatic sulfide deposits in the Emeishan large igneous province, SW China. Chem. Geol. 253, 38–49.
Song, X.Y., Qi, H.W., Hu, R.Z., Chen, L.M., Yu, S.Y., Zhang, J.F., 2013. Formation of thick stratiform Fe–Ti oxide layers in layered intrusion and frequent replenishment of fractionated mafic magma: evidence from the Panzhihua intrusion, SW China. Geochem. Geophys. Geosyst. 14, 712–732.
Tang, Q.Y., Li, C., Tao, Y., Ripley, E.M., Xiong, F., 2017. Association of Mg-rich olivine with Fe-Ti oxides as a result of brucite marble assimilation by basaltic magma in the Emeishan Large Igneous Province, SW China. J. Petrol. 58, 699–714.
Tao, Y., Ma, Y.S., Miao, L.C., Zhu, F.L., 2009. SHRIMP U-Pb zircon age of the Jinbaoshan ultramafic intrusion, Yunnan Province, SW China. Chin. Sci. Bull. (English Edition) 54, 168–172.
Tao, Y., Putirka, K., Hu, R.Z., Li, C., 2015. The magma plumbing system of the Emeishan large igneous province and its role in basaltic magma differentiation in a continental setting. Am. Mineral. 100, 2509–2517.
Toplis, M.J., Carroll, M.R., 1996. Differentiation of ferro-basaltic magmas under conditions open and closed to oxygen: Implications for the Skaergaard intrusion and other natural systems. J. Petrol. 37, 837–858.
Vantongeren, J.A., Mathez, E.A., 2012. Large-scale liquid immiscibility at the top of the Bushveld Complex, South Africa. Geology 40, 491–494.
Veksler, I.V., 2009. Extreme iron enrichment and liquid immiscibility in mafic intrusions: experimental evidence revisited. Lithos 111, 72–82.
Veksler, I.V., Dorfman, A.M., Borisov, A.A., Wirth, R., Dingwell, D.B., 2007. Liquid immiscibility and the evolution of basaltic magma. J. Petrol. 48, 2187–2210.
Viccaro, M., Giacomoni, P.P., Ferlito, C., Cristofolini, R., 2010. Dynamics of magma supply at Mt. Etna volcano (Southern Italy) as revealed by textural and compositional features of plagioclase phenocrysts. Lithos 116, 77–91.
Wang, C.Y., Zhou, M.-F., Zhao, D.G., 2008. Fe–Ti–Cr oxides from the Permian Xinjie mafic–ultramafic layered intrusion in the Emeishan large igneous province, SW China: crystallization from Fe- and Ti-rich basaltic magmas. Lithos 102, 198–217.
Wang, C.Y., Zhou, M.-F., 2013. New textural and mineralogical constraints on the origin of the Hongge Fe–Ti–V oxide deposit, SW China. Miner. Deposita 48, 787–798.
Wang, C.Y., Wei, B., Zhou, M.-F., Minh, D.H., Qi, L., 2018a. A synthesis of magmatic Ni-Cu-(PGE) sulfide deposits in the ~260 Ma Emeishan large igneous province, SW China and northern Vietnam. J. Asian Earth Sci. 154, 162–186.
Wang, K., Wang, C.Y., Ren, Z.Y., 2018b. Apatite-hosted melt inclusions from the Panzhihua gabbroic layered intrusion associated with giant Fe-Ti oxide deposit in SW China: insights for magma unmixing within a crystal mush. Contrib. Miner. Petrol. 173, 59.
Wang, K., Ren, Z.Y., Zhang, L., Ou, Q., 2020. The relationship between the Taihe Fe-Ti oxide ore-bearing layered intrusion and the adjacent peralkaline A-type granitic pluton in SW China: Constraints from compositions of amphiboles and apatite-hosted melt Inclusions. Ore Geol. Rev. 120, 103418.
Xing, C.M., Wang, C.Y., Zhang, M.J., 2012. Volatile and C-H-O isotopic compositions of giant Fe-Ti-V oxide deposits in the Panxi region and their implications for the sources of volatiles and the origin of Fe-Ti oxide ores. Sci. China Earth Sci. 55, 1782–1795.
Xing, C.M., Wang, C.Y., Tan, W., 2017. Disequilibrium growth of olivine in mafic magmas revealed by phosphorus zoning patterns of olivine from mafic-ultramafic intrusions. Earth Planet. Sci. Lett. 479, 108–119.
Xu, Y.G., Chung, S.-L., Jahn, B.M., Wu, G.Y., 2001. Petrological and geochemical constraints on the petrogenesis of the Permo-Triassic Emeishan flood basalts in southwestern China. Lithos 58, 145–168.
Xu, Y.G., He, B., Chung, S.-L., Menzies, M.A., Frey, F.A., 2004. Geologic, geochemical, and geophysical consequences of plume involvement in the Emeishan flood-basalt province. Geology 32, 917–920.
Yu, S.Y., Song, X.Y., Ripley, E.M., Li, C., Chen, L.M., She, Y.W., Luan, Y., 2015. Integrated O-Sr–Nd isotope constraints on the evolution of four important Fe–Ti oxide ore-bearing mafic–ultramafic intrusions in the Emeishan large igneous province, SW China. Chem. Geol. 401, 28–42.
Yu, S.Y., Chen, L.M., Lan, J.B., He, Y.S., Chen, Q., Song, X.Y., 2020. Controls of mantle source and condition of melt extraction on generation of the picritic lavas from the Emeishan large igneous province, SW China. J. Asian Earth Sci. 203, 104534.
Zhang, Z.C., Mahoney, J.J., Mao, J.W., Wang, F.S., 2006. Geochemistry of picritic and associated basalt flows of the western Emeishan flood basalt province, China. J. Petrol. 47, 1997–2019.
Zhang, Z.C., Mao, J.W., Saunders, A.D., Ai, Y., Li, Y., Zhao, L., 2009. Petrogenetic modeling of three mafic–ultramafic layered intrusions in the Emeishan large igneous province, SW China, based on isotopic and bulk chemical constraints. Lithos 113, 369–392.
Zhong, H., Zhu, W.G., 2006. Geochronology of layered mafic intrusions from the Pan-Xi area in the Emeishan large igneous province, SW China. Miner. Deposita 41, 599–606.
Zhong, H., Zhu, W.G., Hu, R.Z., Xie, L.W., He, D.F., Liu, F., Chu, Z.Y., 2009. Zircon U-Pb age and Sr–Nd–Hf isotope geochemistry of the Panzhihua A-type syenitic intrusion in the Emeishan large igneous province, southwest China and implications for growth of juvenile crust. Lithos 110, 109–128.
Zhong, H., Campbell, I.H., Zhu, W.G., Allen, C.M., Hu, R.Z., Xie, L.W., He, D.F., 2011. Timing and source constraints on the relationship between mafic and felsic intrusions in the Emeishan large igneous province. Geochim. Cosmochim. Acta 75, 1374–1395.
Zhou, M.-F., Malpas, J., Song, X.Y., Robinson, P.T., Sun, M., Kennedy, A.K., Lesher, C.M., Keays, R.R., 2002. A temporal link between the Emeishan large igneous province (SW China) and the end-Guadalupian mass extinction. Earth Planet. Sci. Lett. 196, 113–122.
Zhou, M.-F., Robinson, P.T., Lesher, C.M., Keays, R.R., Zhang, C.J., Malpas, J., 2005. Geochemistry, petrogenesis and metallogenesis of the Panzhihua gabbroic layered intrusion and associated Fe–Ti–V oxide deposits, Sichuan Province, SW China. J. Petrol. 46, 2253–2280.
Zhou, M.-F., Arndt, N.T., Malpas, J., Wang, C.Y., Kennedy, A.K., 2008. Two magma series and associated ore deposit types in the Permian Emeishan large igneous province, SW China. Lithos 103, 352–368.
Zhou, M.-F., Chen, W.T., Wang, C.Y., Prevec, S.A., Liu, P.-P., Howarth, G.H., 2013. Two stages of immiscible liquid separation in the formation of Panzhihua-type Fe–Ti–V oxide deposits, SW China. Geosci. Front. 4, 481–502.